Structural and magnetic studies of Cu-doped ZnO films synthesized *via* a hydrothermal route

Tong Li, Haiming Fan, Jiabao Yi, Tun Seng Herng, Yuwei Ma, Xuelian Huang, Junmin Xue and Jun Ding*

Received 19th April 2010, Accepted 13th May 2010
First published as an Advance Article on the web 3rd June 2010
DOI: 10.1039/c0jm01100b

Highly-textured *n*-type ZnO:Cu films with room-temperature ferromagnetism have been hydrothermally grown in aqueous solution at 90 °C using PLD-derived ZnO seed layers on different substrates (quartz, silicon, glass and sapphire). The crystallinity of the ZnO seed layers on different substrates plays an important role in the microstructure of the subsequently grown ZnO:Cu films. Better crystallinity and texture of the seed layers is favourable to the growth of continuous films. Thick $Zn_{0.98}Cu_{0.02}O$ films (*ca.* 1.2 μm) exhibit high value of magnetic moment (0.40 μ_B per Cu), comparable to the previously reported value of thin films, indicating that thick ZnO:Cu films with high magnetization can be synthesized *via* this hydrothermal route. The incorporation of hydrogen into the ZnO lattice plays a dominant role in ferromagnetism in this ZnO:Cu system.

1. Introduction

Diluted magnetic semiconductors (DMSs) have recently drawn considerable attention for their novel applications in spintronics.[1–3] Both theoretical[4] and experimental[5–7] studies showed that transition metal (TM) doped ZnO materials are of particular interest because these are potential DMSs with a high Curie temperature above room temperature. However, the origin of the ferromagnetism in ZnO-based DMS materials was plagued by the precipitates, clustering or secondary phase of doped magnetic elements.[8,9] In this context, Cu-doped ZnO have provoked broad interest and this is mostly because neither metallic copper nor its compounds are ferromagnetic. Indeed, first-principle calculations showed that the ZnO:Cu system possesses a ferromagnetic state.[10] Experimental observations of room temperature ferromagnetism (RTF) in Cu-doped ZnO materials further confirmed this theoretical prediction.[11–13] Additionally, a thick film with relatively strong ferromagnetism is favourable for the study on the origin of ferromagnetism in ZnO:TM because it can exclude the possibility of strain-induced ferromagnetism enhancement[14] related to thin films and reduce the possibility of contamination signal during sample transport and handling.

Recently, some studies have been focused on the influence of hydrogen on the ferromagnetic properties of ZnO:TM.[15–19] This was firstly motivated by the fact that H can be inevitably introduced during crystal growth or device processing.[20–22] In addition, it has lately been found that ferromagnetism can be activated in ZnO:TM *via* heat treatment in a hydrogen environment.[15,16] Theoretical studies have predicted that H can mediate ferromagnetic spin–spin interaction between neighboring TM impurities. H-induced carriers may also play important roles in the magnetic properties of the ZnO:TM system.

Department of Materials Science and Engineering, Faculty of Engineering, National University of Singapore, Singapore 117574. E-mail: msedingj@nus.edu.sg; Fax: +65 67763604; Tel: +65 65164317

In existing deposition techniques for ZnO and ZnO:TM, the low temperature aqueous synthesis such as hydrothermal method has aroused substantial interest due to its great advantages in low cost and especially in green environmental protection.[23,24] In recent years, Lange *et al.*[23–25] have demonstrated the ability of synthesizing epitaxial ZnO films from aqueous solutions at temperatures as low as 90 °C. Zhang *et al.*[18] then employed a hydrothermal method to successfully prepare epitaxial ZnO:Co films with room-temperature ferromagnetism. Hydrogen can be incorporated into the ZnO lattice more easily when exposed to ambient water.[26] Goh *et al.*[27,28] have found that hydrogen is incorporated into the lattice of hydrothermally synthesized oxides as hydroxyl ions. It is thus necessary to figure out the effect of hydrogen on magnetic properties of ZnO:TM prepared *via* a hydrothermal route.

In this study, highly-textured thick Cu-doped ZnO films (n type) with high room-temperature ferromagnetism have been synthesized by a hydrothermal route using PLD-derived ZnO seed layers. The microstructure of these films was investigated in the dependence of texture of the seed layers on different substrates. In addition, the effect of hydrogen on ferromagnetic properties of this ZnO:Cu system was further figured out.

2. Experimental

Pure ZnO films grown by pulse laser deposition (PLD) on different substrates including quartz, glass, silicon (100) and sapphire (0001) were employed as seed layers to further hydrothermally grow ZnO and Cu-doped ZnO films. The seed layers were approximately 50 nm thick and had (0001) preferred orientation after the deposition at 400 °C. In the hydrothermal process, the precursor solution consists of 0.026 M zinc nitrate hexahydrate (Fluka, 99.9%) and 0.3125 M ammonium nitrate (Sigma Aldrich, 99.9%) and different concentration of copper nitrate trihydrate (Fluka, 99.9%) dissolved in deionized water. The ammonium hydroxide (30%) was then added to adjust the pH value of the precursor solution to 7.5. The substrates with ZnO seed layers were affixed to a Teflon insert and stood upright

in a sealed hydrothermal autoclave, which was placed in an oven at 90 °C for 24 h. The autoclave was then cooled down to room temperature and the specimens were rinsed in deionized water and dried. In this work, we obtained $Zn_{1-x}Cu_xO$ films with different copper concentration $x = 0$, 0.01, 0.02, and 0.05 on different substrates and also corresponding powder samples. Thermal annealing treatments of the as-prepared samples were carried out in different atmosphere including O_2/Ar (20%/80%) atmosphere, pure Ar (99.9999%) atmosphere and H_2/Ar (2.5%/97.5%) atmosphere. In this hydrothermal process, we chose pH = 7.5 as the reaction condition. Our study has found that two pH ranges are favourable to the film formation (7.0–7.5 and 10.5–11), while a pH value in the range of 8.0–9.0 results in a higher powder yield rather than the film. Similar results have been reported previously.[24] Under the lower pH value (~7.5), the ZnO crystallites grow with a flatter (0001) surface, while sharp needle-shaped crystallites are formed with a higher pH value (~10.9).[25,29]

The morphology and composition of the films were investigated by scanning electron microscopy (SEM; XL 30 FEG Philips, Hillsboro, OR) and energy-dispersive X-ray spectroscopy (EDX), respectively. Phase identification and crystal orientation were determined by X-ray diffraction (XRD) (Bruker, Advance D8) using θ–2θ scans and off-axis Φ-scans (Bruker, Discover D8). Optical properties were characterized by UV-visible absorption spectroscopy (Varian Cary 5000) and room temperature PL measurements (Renishaw Invia Micro-PL). The electrical properties were investigated using a Hall Effect system (HL5500PC, BIO-RAD) and four-point probe method. The ferromagnetic behaviours of Cu-doped ZnO films at room temperature were carried out by a vibrating sample magnetometer (VSM; Lakeshore, Model 7407) and a superconducting quantum interference device (SQUID; Quantum Design, MPMS, XL-5). X-Ray photoelectron spectroscopy (XPS; VG ESCALAB 200i-XL) was used in the study of the film composition and ionic states.

3. Results and discussion

3.1 Structural study of ZnO films

As the basic research of our work, the fundamental characteristics of pure ZnO films grown on different substrates were firstly investigated. The surface morphology and cross section SEM images of pure ZnO films grown on quartz, glass, silicon and sapphire substrates are shown in Fig. 1. As shown in Fig. 1(a) and (b), discontinuous ZnO films with a relatively rough surface morphology are shown on quartz and glass substrates, and the film is composed of incompletely coalesced hexagonally shaped ZnO rods (*ca.* 1.5–2 μm in length). In contrast, both ZnO/Si and ZnO/sapphire films (see Fig. 1(c) and Fig. 1(d), respectively) are composed of fully coalesced hexagonal rods (*ca.* 1–1.5 μm in length), displaying a continuous morphology with a smooth surface. The XRD θ–2θ scans of ZnO films on different substrates in Fig. 2(a) shows that the prominent (002) peak corresponding to the ZnO wurtzite structure appears in all of the four films, indicating that the ZnO films are grown with *c*-axis preferred orientation. The rocking curves (RCs) on the (002) reflection of the four samples are shown in the inset of Fig. 2(a).

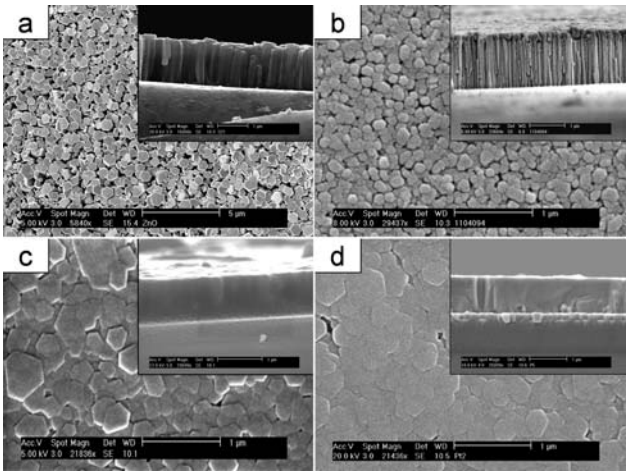

Fig. 1 Field emission SEM images of the surface morphology of (a) ZnO/quartz films; (b) ZnO/glass films; (c) ZnO/Si films; and (d) ZnO/sapphire films. The insets show the corresponding cross-sectional morphology of each film.

The full width half maximum (FWHM) values of RCs for the ZnO seed layers on quartz, glass, Si and sapphire substrates are 1.7, 2.8, 1.5 and 0.9, respectively, indicating that the seed layers fabricated by PLD on Si and sapphire substrates had better crystallinity and texture than those on quartz and glass substrates. It is also interesting to note that the FWHM values were reduced after the hydrothermal process compared to those

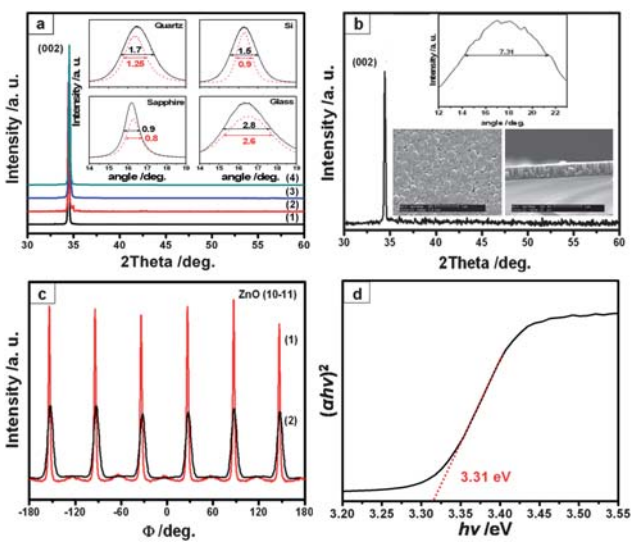

Fig. 2 (a) θ–2θ XRD patterns of ZnO film on quartz (1), silicon (2), sapphire (3) and glass (4) substrates. The inset shows the XRD rocking curves on the (002) reflection of ZnO/quartz, ZnO/sapphire, ZnO/Si, ZnO/glass films (dashed lines) compared with their seed layers (full lines) fabricated by PLD, respectively. (b) θ–2θ XRD patterns of ZnO film on amorphous ZnO/quartz substrates. The insets show the XRD rocking curves on its (002) reflection and the surface and cross sectional morphology of the film. (c) Off-axis Φ-scan for (101) plane of (1) ZnO/sapphire and (2) ZnO/quartz films. (d) $(\alpha h\nu)^2$ plotted against the photon energy $h\nu$ based on the UV-visible absorption spectra of ZnO/quartz films.

of the seed layers. It thus suggests that the crystallinity of the ZnO seed layers grown on different substrates plays an important role in the microstructure of the subsequently grown ZnO films derived from the hydrothermal process. A better crystallinity and texture of the seed layers is favourable to the growth of continuous films. To further confirm the effect of crystallinity of seed layers on film morphology, the amorphous ZnO seed layer fabricated on quartz by PLD deposited at room temperature was employed to hydrothermally grow ZnO film. As shown in Fig. 2(b), although this film also shows a (002) texture, the FWHM value is very large (7.31°) with a columnar structure.

Furthermore, the off-axis Φ-scan for (101) planes of ZnO films in Fig. 2(c) shows that both ZnO/quartz and ZnO/sapphire films exhibit peaks with six-fold symmetry corresponding to the wurtzite structure, indicating the presence of epitaxial in-plane alignment. However, it is also clear that compared with the ZnO/sapphire film, the peaks for the ZnO/quartz film show larger FWHM values (10–12°) and much lower intensity, indicating that the epitaxial in-plane texture is much weaker in the ZnO/quartz film and it could be attributed to the relatively large lattice mismatch between ZnO and quartz. In addition, the off-axis Φ-scan for (101) planes of ZnO/Si and ZnO/glass films shows no peaks, revealing that the in-plane orientation has random distribution (no epitaxial growth). As reported in our previous work,[30,31] the ZnO film fabricated by PLD may have an epitaxial growth on quartz and sapphire substrates, while ZnO can only have the (002) texture on Si and glass substrates.

In addition, Fig. 2(d) shows the plot of $(\alpha h\nu)^2$ against the photon energy $h\nu$ based on the room temperature UV-visible absorption spectra of ZnO/quartz films. It shows that the bandgap energy of ZnO film is 3.31 eV, which is consistent with the reported values (3.24–3.3 eV) of ZnO films prepared by different techniques.[32,33] It is also found that the ZnO/glass, ZnO/Si and ZnO/sapphire films have similar values of bandgap energy as that of the ZnO/quartz film. In addition, the Hall measurement shows that as-deposited ZnO/quartz, ZnO/glass, ZnO/Si and ZnO/sapphire films all exhibit n-type conduction with carrier concentration of $\sim 4 \times 10^{18}$ cm^{-3} and carrier mobility of 20–30 $cm^2\ V^{-1}\ s^{-1}$ (Table 1), which are comparable to the values reported for hydrothermally grown ZnO films by Andeen *et al.*[29]

3.2 Structural and magnetic study of Cu-doped ZnO films

3.2.1 Doping concentration. The microstructure of Cu-doped ZnO films also depends on a similar substrate effect as that of pure ZnO films. According to SEM images of surface and cross sectional morphology of $Zn_{0.98}Cu_{0.02}O$ films on quartz, Si and sapphire substrates shown in Fig. 3(a)–(f), the Cu-doped ZnO films on different substrates show different morphologies. On quartz substrates, a relatively rough film with discontinuous columnar structures is formed, while on Si substrates, especially on sapphire substrates, it forms continuous films with a quite smooth surface. The EDX spectra shown in the inset of Fig. 3(a), (c) and (e) confirm that the composition of these films is $Zn_{0.98}Cu_{0.02}O$ and no other elements are present except for the Au peak due to the Au coating for the SEM examination.

$Zn_{1-x}Cu_xO$ films with different copper atomic concentrations $x = 0$, 0.01, 0.02, and 0.05 were hydrothermally grown on quartz substrates. The X-ray diffraction patterns of the $Zn_{1-x}Cu_xO$ films are displayed in Fig. 4 (a). All of them exhibit a prominent (002) peak corresponding to the wurtzite structure and no other diffraction peaks are detected, revealing the single ZnO wurtzite phase with a *c*-axis preferred orientation. Moreover, the (002) peak is at 34.44°, 34.46°, 34.50°, and 34.52° for ZnO, $Zn_{0.99}Cu_{0.01}O$, $Zn_{0.98}Cu_{0.02}O$, and $Zn_{0.95}Cu_{0.05}O$ films, respectively, indicating the reduction of lattice constant *c* with increasing copper concentration. It confirms the substitution of Zn^{2+} by Cu^{2+} due to the smaller size of Cu^{2+} (Cu^{2+} ions have radii of 0.057 nm as compared to 0.06 nm for Zn^{2+} ions).[34] The inset in

Table 1 Resistivity, carrier concentration and carrier mobility of $Zn_{1-x}Cu_xO$/quartz films with $x = 0$, 1%, 2% and 5%

	Samples	Resistivity/ Ω cm	Carrier conc./cm^{-3}	Carrier mobility/ $cm^2\ V^{-1}\ s^{-1}$
ZnO films	Pure ZnO on quartz/Si/ sapphire	0.05	-4×10^{18}	20–30
$Zn_{1-x}Cu_xO$/ quartz films	$Zn_{0.99}Cu_{0.01}O$	0.21	-7.26×10^{17}	10.9
	$Zn_{0.98}Cu_{0.02}O$	0.44	-6.78×10^{17}	12.4
	$Zn_{0.95}Cu_{0.05}O$	1.08	-2.31×10^{17}	11.3

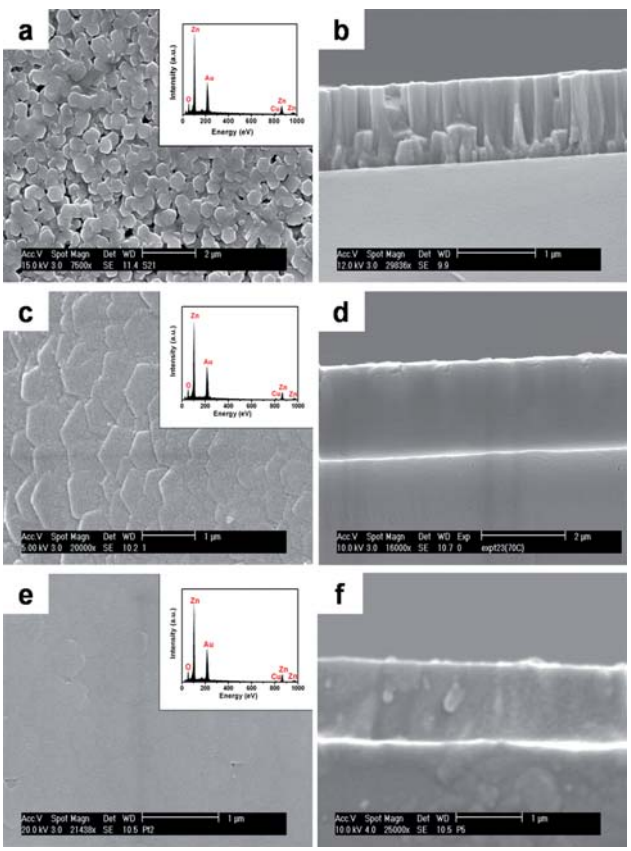

Fig. 3 Field emission SEM images of (a) surface morphology and (b) cross section of $Zn_{0.98}Cu_{0.02}O$/quartz films, (c) surface morphology and (d) cross section of $Zn_{0.98}Cu_{0.02}O$/Si films, and (e) surface morphology and (f) cross section of $Zn_{0.98}Cu_{0.02}O$/Sapphire films. The insets in (a), (c) and (e) are EDX spectra of $Zn_{0.98}Cu_{0.02}O$/quartz, $Zn_{0.98}Cu_{0.02}O$/Si and $Zn_{0.98}Cu_{0.02}O$/Sapphire films, respectively.

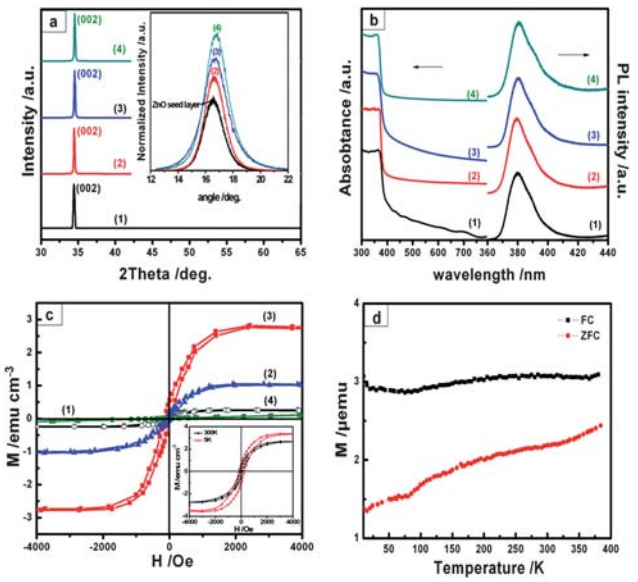

Fig. 4 (a) θ–2θ XRD patterns of $Zn_{1-x}Cu_xO$/quartz films. The inset shows the XRD rocking curves on the (002) reflection of $Zn_{1-x}Cu_xO$ film and the pure ZnO seed layer fabricated by PLD. (b) The UV-visible absorption spectra and normalized room-temperature PL spectra of $Zn_{1-x}Cu_xO$ films. (c) Magnetization *versus* magnetic field (*M*–*H*) loops for $Zn_{1-x}Cu_xO$ films at room temperature. The bottom right inset shows the *M*–*H* loops for $Zn_{0.98}Cu_{0.02}O$/quartz films at 5 K and 300 K. (d) Temperature dependence of FC and ZFC magnetizations for $Zn_{0.98}Cu_{0.02}O$/quartz films. Here, (1), (2), (3), and (4) represent the $Zn_{1-x}Cu_xO$ films with $x = 0$, 0.01, 0.02 and 0.05, respectively.

Fig. 4 (a) shows the X-ray diffraction rocking curves (RCs) on the (002) reflection of the samples. The typical FWHM values are around 1.6° for the pure ZnO seed layer in contrast to 1.7°, 1.9°, and 2.0° for $Zn_{0.99}Cu_{0.01}O$, $Zn_{0.98}Cu_{0.02}O$, and $Zn_{0.95}Cu_{0.05}O$, respectively. The increase in FWHM value might be related to the increase in structural disorder with increasing Cu concentration. Our EDX and XPS results revealed the existence of Cu, Zn, and O in these samples. No other elements or impurities could be found. It is also confirmed that the Cu content in films is very close to the nominal content in their precursor solution.

In Fig. 4(b), the UV-visible spectra exhibit red shifts of 1.25, 3.60, 8.20 nm for $Zn_{0.99}Cu_{0.01}O$, $Zn_{0.98}Cu_{0.02}O$, and $Zn_{0.95}Cu_{0.05}O$, respectively, compared to ZnO (at about 372 nm), indicating a bandgap reduction.[35,36] Additionally, in the PL spectra, a near band-edge emission (NBE) appears at 376 nm in the ultraviolet spectral region for ZnO. After doping, the NBE peak shifts towards longer wavelength with increasing Cu concentration, which arises from the decrease of bandgap due to strong coupling between localized 3d electrons of Cu^{2+} and the extended s and p carriers of ZnO.[37] The results further confirm that copper dopants are incorporated into the ZnO host lattice.

Fig. 4(c) depicts the typical magnetization *versus* magnetic field (*M*–*H*) loops for Cu-doped ZnO films at room temperature. As shown, no ferromagnetism can be detected from pure ZnO. However, a well defined hysteresis behaviour observed in $Zn_{0.99}Cu_{0.01}O$, $Zn_{0.98}Cu_{0.02}O$, and $Zn_{0.95}Cu_{0.05}O$ indicates that Cu-doped ZnO films exhibit RTF. The saturated magnetization of $Zn_{0.99}Cu_{0.01}O$, $Zn_{0.98}Cu_{0.02}O$, and $Zn_{0.95}Cu_{0.05}O$ are 1.02, 2.75, and 0.26 emu cm^{-3}, respectively. Using the actual Cu content in the Cu-doped ZnO films, the Cu moment was computed to be around 0.28, 0.40, and 0.01 μ_B/Cu for $x = 0.01$, 0.02, and 0.05, respectively. Cu in the $Zn_{0.98}Cu_{0.02}O$ sample has the highest moment value. Liu *et al.*[14] has found that the saturated magnetization of Co-doped ZnO films could rapidly decrease with increasing film thickness from 15 nm to 900 nm due to the decrease of lattice strain. However, in our work, the $Zn_{0.98}Cu_{0.02}O$ film with a thickness of 1.2 μm exhibits comparable saturated magnetization with previously reported 250 nm-thick Cu-doped ZnO films (~0.4 μ_B/Cu),[38] which indicates that we could obtain thick films with high magnetization *via* this hydrothermal process. This result also confirms that the ferromagnetism is originated from Cu doping but not strain. It can also been found from *M*–*H* loops that as the Cu concentration increases from 0.02 to 0.05, the magnetic moment per Cu ion markedly decreases. Theoretical study of the ZnO:Cu system indicated that the relative location of the Cu atoms to each other can strongly affect its magnetic properties. Feng[39] suggested that for the case where Cu atoms were separated by 5.2424 Å along the *c*-axis the ferromagnetic state was favoured. In contrast, the case where Cu atoms were separated by 3.2587 Å within the *ab* plane would lead to an antiferromagnetic state. Therefore, for our samples, the decrease in magnetic moment per Cu ion could be attributed to an increased number of copper atoms occupying adjacent cation positions resulting in antiferromagnetic alignment. The bottom right inset in Fig. 4(c) shows the *M*–*H* loops conducted at 5 K and 300 K for $Zn_{0.98}Cu_{0.02}O$/quartz film. The coercivity of the film at 5 K and 300 K is 202 Oe and 70 Oe, respectively. The relatively large coercivity confirms the ferromagnetic coupling. In addition, the zero-field-cooled (ZFC) and field cooled (FC) magnetization curves in the temperature range of 10–300 K at a magnetic field of 500 Oe on $Zn_{0.98}Cu_{0.02}O$/quartz film in Fig. 4(d) further confirm the ferromagnetism of the sample with a Curie temperature over 400 K.

Hall measurements indicate that Cu-doped ZnO films with different Cu concentrations all exhibit n-type conductivity. It is known that pure ZnO film normally shows n-type conductivity. The n-type conductivity of ZnO originates from a combination effect of Zn interstitial, oxygen vacancy, and hydrogen atoms unintentionally incorporated during the preparation process.[40] Compared with the carrier concentration of pure ZnO film, doping of Cu reduces the effective number of n-type carriers in the system, as shown in Table 1. It may be attributed to the incorporation of holes in the film due to Cu doping.[41] However, the overall nature of the films remains n-type. In addition, $Zn_{0.95}Cu_{0.05}O$ film has lower carrier concentration (2.31×10^{17} cm^{-3}) than that of $Zn_{0.99}Cu_{0.01}O$ (7.26×10^{17} cm^{-3}) and $Zn_{0.98}Cu_{0.02}O$ (6.78×10^{17} cm^{-3}). Therefore, besides the copper ions antiferromagnetic coupling, the decrease in carrier concentration may also contribute to the lower saturation magnetization for the doping with higher Cu content. The electrical resistivity measured by the four-point probe method increases with increasing Cu concentration in Cu-doped ZnO film, as shown in Table 1.

3.2.2 Annealing effect. In order to understand the origin of ferromagnetism in ZnO:Cu films, the deposited films were performed annealing under different atmospheres. Fig. 5(a) shows room temperature PL spectra of as-prepared

$Zn_{0.98}Cu_{0.02}O$/quartz film and the films annealed in O_2/Ar (20%/80%), H_2/Ar (2.5%/97.5) and a pure Ar environment. A strong deep level broad emission (DLE) band is observed for the as-prepared film, which may be attributed to the presence of a considerable amount of oxygen interstitials, oxygen vacancies, Zn vacancies and Zn interstitials.[42–44] For the film annealing under O_2/Ar, the DLE band is still obviously observed, though the intensity is reduced. For the film annealed under H_2/Ar, the DLE band disappears and the NBE intensity increases by more than ten times, probably due to the passivation of deep-level states by hydrogen.[45] For the film annealed under pure Ar, the shift towards the green emission region of the DLE band center position may be due to the increased amount of oxygen vacancies. Fig. 5(b) shows *M–H* loops of as-prepared and annealed samples. It can be seen that the saturation magnetization of the sample after annealing in H_2/Ar is not decreased but is comparable to that of the as-prepared one. For the $Zn_{0.98}Cu_{0.02}O$/quartz film annealed in O_2/Ar atmosphere, the saturation magnetization is drastically decreased from 2.4 emu cm^{-3} (0.35 μ_B/Cu) to 0.1 emu cm^{-3} (0.015 μ_B/Cu). In addition, for the film annealed in pure Ar, the saturation magnetization is decreased to 1.6 emu cm^{-3} (0.24 μ_B/Cu). These results suggest that ferromagnetism in ZnO:Cu is not mainly mediated by electron carriers induced by structural defects (*i.e.* oxygen vacancy).

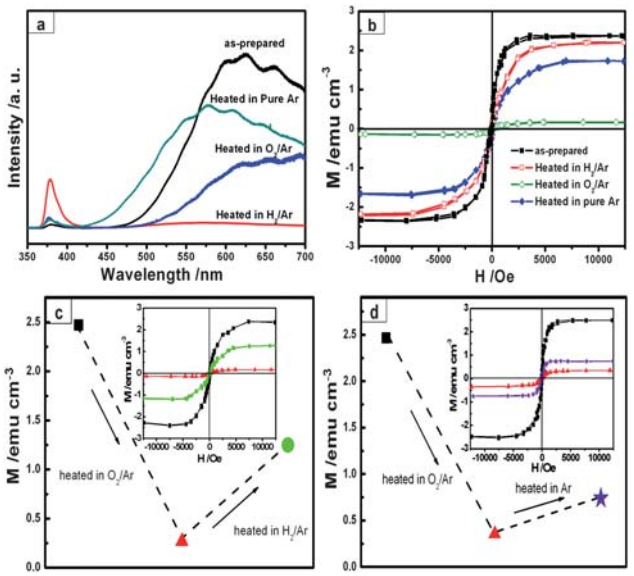

Fig. 5 (a) Room-temperature PL spectra and (b) Magnetization *versus* magnetic field (*M–H*) loops for as-prepared $Zn_{0.98}Cu_{0.02}O$/quartz film, the film annealed at 600 °C in H_2/Ar (2.5%/97.5%) atmosphere for 1 h, the film annealed at 600 °C in O_2/Ar (20%/80%) atmosphere for 1 h, and the film annealed at 600 °C in pure Ar for 1 h. (c) Variation of saturation magnetization of $Zn_{0.98}Cu_{0.02}O$ film while heated at 600 °C in O_2/Ar (20%/80%) atmosphere for 1 h and then in H_2/Ar (2.5%/97.5%) atmosphere at 600 °C for 1 h. (d) Variation of saturation magnetization of $Zn_{0.98}Cu_{0.02}O$ film while heated at 600 °C in O_2/Ar (20%/80%) for 1 h and then in pure Ar atmosphere at 600 °C for 1 h. The insets in (c) and (d) show the corresponding *M–H* loops. Here, ■ represents the as-prepared samples, ▲ represents the samples heated in O_2/Ar atmosphere, ● represents the samples heated in O_2/Ar atmosphere and then in H_2/Ar atmosphere, and ★ represents the samples heated in O_2/Ar atmosphere and then in pure Ar atmosphere.

In order to further understand the mechanism of ferromagnetism in the ZnO:Cu system, a cycling annealing under an O_2 and a H_2 environment alternately was conducted for $Zn_{0.98}Cu_{0.02}O$/quartz film. As shown in Fig. 5 (c), it can be noted that annealing in O_2/Ar (20%/80%) atmosphere results in drastic decrease of saturation magnetization from 2.4 emu cm^{-3} to 0.1 emu cm^{-3}. However, subsequent annealing under H_2 atmosphere recovers the ferromagnetism up to 1.25 emu cm^{-3} (0.18 μ_B per Cu). The corresponding transport properties for these cycling annealed samples are shown in Table 2. It can be seen that after annealing under O_2/Ar atmosphere, the resistivity is markedly increased from 0.44 Ω cm to 1270 Ω cm, and thus the carrier concentration decreases to a very low level. (The low carrier concentration is beyond our system limitation and cannot be detected.) When the annealed sample was subsequently annealed in H_2/Ar, the resistivity was decreased to 1.25 Ω cm and carrier concentration was increased to 3.17×10^{18} cm^{-3}. In addition, a cycling annealing in O_2 environment and subsequently in pure Ar was also carried out for $Zn_{0.98}Cu_{0.02}O$/quartz film. Fig. 5(d) shows that subsequent annealing under a pure Ar atmosphere can only slightly recover the ferromagnetism. The resistivity was decreased to 350 Ω cm, whereas, we still cannot measure the carrier concentration due to equipment limitation. Similar results to that of ZnO:Cu/quartz films were obtained when a cycle annealing process as shown above was conducted for ZnO:Cu/Si and ZnO:Cu/sapphire films. These results suggest that hydrogen may play an important role in the ferromagnetism of the ZnO:Cu system. Park and Chadi[19] have employed first principles pseudopotential calculations to predict that H can mediate a strong short-ranged ferromagnetic spin–spin interaction between neighboring TM impurities through the formation of a bridge bond. Lee *et al.*[15] have experimentally shown that the robust ferromagnetism of ZnCoO after being hydrogenated in Ar/H_2 mixed gas is due to the enhancement of ferromagnetic spin–spin interaction in the H–Co coupling. In addition, it is well documented that when the introduction of H into ZnO from a H_2 ambient is carried out at elevated temperature, stable carrier are generated.[21] Park *et al.*[17] have found that the H-induced carriers play important roles in the magnetic properties of hydrogenated ZnMnO films. Furthermore, H incorporation is often observed in hydrothermally synthesized materials. Zhang *et al.*[46] have hydrothermally prepared epitaxial ZnCoO films with room-temperature ferromagnetism which is attributed to hydrogen unintentionally incorporated in the aqueous route by enhancing

Table 2 Resistivity, carrier concentration and carrier mobility of $Zn_{0.98}Cu_{0.02}O$/quartz films under different annealing conditions

Samples	Resistivity/ Ω cm	Carrier conc./cm^{-3}	Carrier mobility/ $cm^2\ V^{-1}\ s^{-1}$
As-prepared $Zn_{0.98}Cu_{0.02}$ film	0.44	-6.78×10^{17}	12.4
Heated in O_2/Ar	1270	NA	NA
Heated in O_2/Ar, and then in H_2/Ar	1.25	-3.17×10^{18}	23.4
Heated in O_2/Ar, and then in pure Ar	350	NA	NA

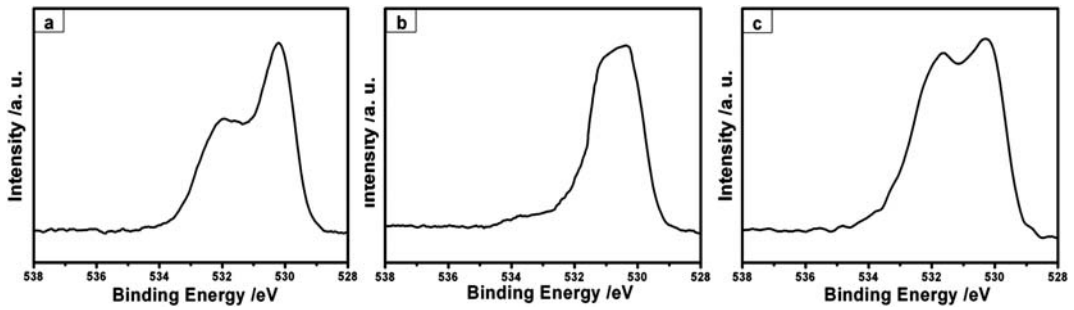

Fig. 6 O 1s XPS spectra for (a) the as-prepared $Zn_{0.98}Cu_{0.02}O$ films, (b) the films annealed in O_2/Ar (20%/80%) atmosphere and (c) the films annealed in O_2/Ar (20%/80%) atmosphere and subsequently in H_2/Ar (2.5%/97.5%) environment.

carrier concentration as a shallow donor. In view of the above factors, the incorporation of hydrogen into ZnO lattice is the dominant effect on the enhancement of ferromagnetism in our ZnO:Cu system. The incorporation of hydrogen may either act as a bridge bond for Cu ions to enhance their spin–spin interaction or provide electron carriers to mediate room temperature ferromagnetism.

Fig. 6 shows the O 1s XPS spectra for as-prepared and annealed samples. The main peak centered at 530.2 eV is attributed to the O 1s core level in the ZnO wurtzite structure surrounded by the Zn atoms with their full complement of nearest-neighbour oxygen ions.[47] The peak at higher binding energy around 531.5 eV is associated with hydroxidic oxygen.[48] The as-prepared film exhibits the ratio of O (hydroxide) : O (oxide) ~2 : 5. For the film annealing under O_2/Ar, the hydroxide peak becomes insignificant. When the annealed sample was subsequently annealed in H_2/Ar, the hydroxide peak grew to a very larger extent. In this case the peak ratio is grew up to O (hydroxide) : O (oxide) ~2 : 3. Hydroxyl ions have been found to incorporate into the lattice of hydrothermally synthesized oxides. It has been observed that the IR absorption peak arised from O–H complexes in ZnO after annealing in a H_2 environment.[21,49] The XPS results confirm the presence of hydrogen, possibly incorporated in the lattice as hydroxyl groups.

In order to confirm the effect of hydrogen on the magnetic properties of ZnO:Cu, we synthesized $Zn_{0.98}Cu_{0.02}O$ powder-like

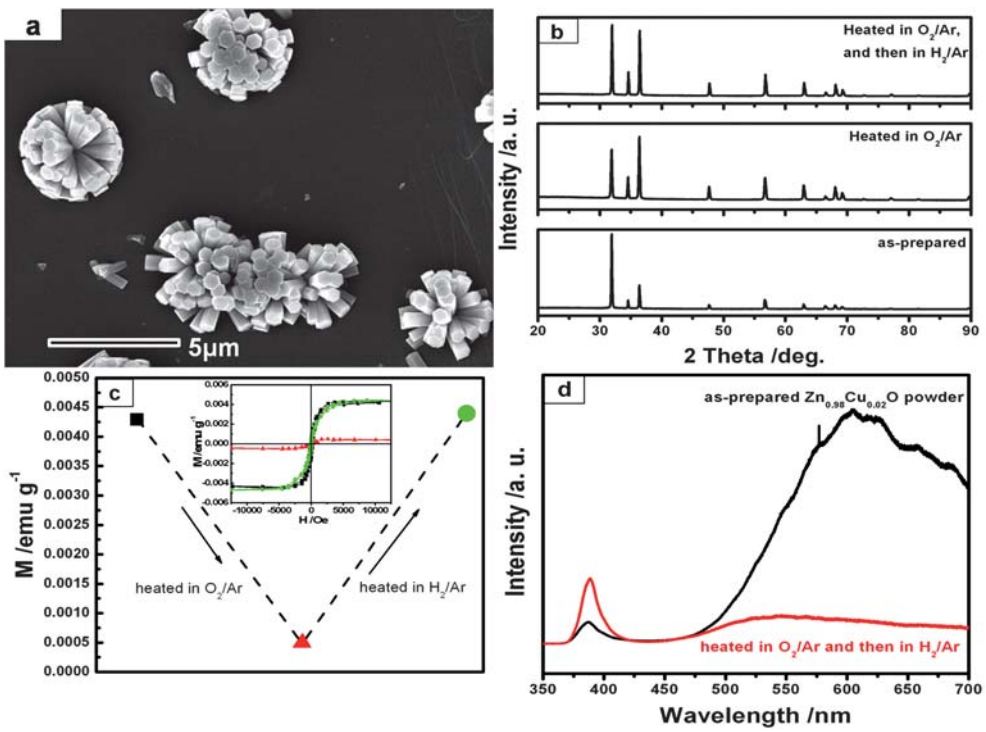

Fig. 7 (a) SEM images of $Zn_{0.98}Cu_{0.02}O$ powders prepared by a hydrothermal route with pH = 7.5. (b) XRD spectra of $Zn_{0.98}Cu_{0.02}O$ powders while heated in different atmospheres. (c) Variation of saturated magnetization of $Zn_{0.98}Cu_{0.02}O$ powders while heated in different atmospheres. The inset in (c) shows the corresponding *M–H* loops. Here, ■ represents the as-prepared powders, ▲ represents the powders heated at 600 °C in O_2/Ar (20%/80%) atmosphere for 1 h, and ● represents the powders heated at 600 °C in O_2/Ar (20%/80%) atmosphere and then in H_2/Ar (2.5%/97.5%) atmosphere at 600 °C for 1 h. (d) Room-temperature PL spectra of as-prepared $Zn_{0.98}Cu_{0.02}O$ powders and the powders heated at 600 °C in O_2/Ar (20%/80%) atmosphere and then in H_2/Ar (2.5%/97.5%) atmosphere at 600 °C for 1 h.

samples *via* a similar hydrothermal process and also conducted a similar cycling annealing under O_2 and H_2 environment to confirm that the ferromagnetism in ZnO:Cu is related to the incorporation of hydrogen. The SEM image of the as-prepared $Zn_{0.98}Cu_{0.02}O$ powders in Fig. 7(a) shows the typical flower-like ZnO composed of rods. The individual ZnO rods clearly reveal the regular hexagonal structure. The typical XRD patterns of as-prepared powders as well as the ones undergoing cycling annealing are shown in Fig. 7(b). It indicates that all peaks correspond to a ZnO hexagonal wurtzite structure and no secondary phase or metal-related peak can be detected after annealing. Fig. 7(c) shows the magnetic behavior of the powders after cycling annealing. Similarly, annealing in O_2/Ar atmosphere of the powders leads to a drastic decrease of saturation magnetization from 0.0043 to 0.0005 emu g^{-1}. A subsequent annealing of the annealed powders in H_2/Ar recovers the saturation magnetization to 0.0044 emu g^{-1}, almost the same as that of as-prepared powders. From PL spectra in Fig. 7(d), the crystal quality is strongly improved after the cycling annealing process. Therefore, both the results on film samples and powder samples demonstrate that the incorporation of hydrogen into the ZnO lattice plays an important role in the ferromagnetism of the ZnO:Cu system.

4. Conclusion

In summary, highly-textured n-type Cu-doped ZnO films (*ca.* 1.2 μm) with high room-temperature ferromagnetism have been synthesized by a hydrothermal route using PLD-derived ZnO seed layers. The structural study revealed that the microstructure and surface morphology of the hydrothermally grown films are dependent on the microstructure of PLD-derived seed layers on different substrates. High-quality seed layers are favourable to the formation of continuous and smooth films. The enhanced ferromagnetism of this ZnO:Cu system is mainly due to the incorporation of hydrogen in the ZnO lattice, which may provide electron carriers mediating the ferromagnetism.

References

1 S. A. Wolf, D. D. Awschalom, R. A. Buhrman, J. M. Daughton, S. von Molnár, L. M. Roukes, A. Y. Chtchelkanova and D. M. Treger, *Science*, 2001, **294**, 1488.
2 H. Ohno, *Science*, 1998, **281**, 951.
3 K. Ando, *Science*, 2006, **312**, 1883.
4 T. Dietl, H. Ohno, F. Matsukura, J. Gilbert and D. Ferrand, *Science*, 2000, **287**, 1019.
5 S. J. Pearton, D. P. Norton, K. Ip, Y. W. Heo and T. Steiner, *J. Vac. Sci. Technol., B*, 2004, **22**, 932.
6 P. Sharma, A. Gupta, K. V. Rao, F. J. Owens, R. Sharma, R. Ahuja, J. M. O. Guillen, B. Johansson and G. A. Gehring, *Nat. Mater.*, 2003, **2**, 673.
7 Z. L. Lu, H. S. Hsu, Y. H. Tzeng, F. M. Zhang, Y. W. Du and J. C. A. Huang, *Appl. Phys. Lett.*, 2009, **95**, 102501.
8 J. H. Park, M. G. Kim, H. M. Jang, S. Ryu and Y. M. Kim, *Appl. Phys. Lett.*, 2004, **84**, 1388.
9 W. Chen, L. F. Zhao, Y. Q. Wang, J. H. Miao, S. Liu, Z. C. Xia and S. L. Yuan, *Solid State Commun.*, 2005, **134**, 827.
10 L. H. Ye, A. J. Freeman and B. Delley, *Phys. Rev. B: Condens. Matter Mater. Phys.*, 2006, **73**, 033203.
11 K. Ando, H. Saito, Z. Jin, T. Fukumura, M. Kawasaki, Y. Matsumoto and H. Koinuma, *J. Appl. Phys.*, 2001, **89**, 7284.
12 D. B. Buchholz, R. P. H. Chang, J. H. Song and J. B. Ketterson, *Appl. Phys. Lett.*, 2005, **87**, 082504.
13 D. L. Hou, X. J. Ye, H. J. Meng, H. J. Zhou, X. L. Li, C. M. Zhen and G. D. Tang, *Appl. Phys. Lett.*, 2007, **90**, 142502.
14 X. J. Liu, C. Song, F. Zeng, F. Pan, B. He and W. S. Yan, *J. Appl. Phys.*, 2008, **103**, 093911.
15 H. J. Lee, C. H. Park, S. Y. Jeong, K. J. Yee, C. R. Cho, M. H. Jung and D. J. Chadi, *Appl. Phys. Lett.*, 2006, **88**, 062504.
16 O. D. Jayakumar, I. K. Gopalakrishnan, K. Shashikala and S. K. Kulshreshtha, *Appl. Phys. Lett.*, 2006, **89**, 202507.
17 S. Y. Park, S. W. Shin, P. J. Kim, J. H. Kang, T. H. Kim, Y. P. Lee and J. Magn, *J. Magn. Magn. Mater.*, 2007, **310**, e708.
18 Y. B. Zhang, S. Li, G. K. L. Goh and S. Tripathy, *Appl. Phys. Lett.*, 2008, **93**, 102510.
19 C. H. Park and D. J. Chadi, *Phys. Rev. Lett.*, 2005, **94**, 127204.
20 C. G. Van de Walle, *Phys. Rev. Lett.*, 2000, **85**, 1012.
21 G. A. Shi, M. Stavola, S. J. Pearton, M. Thieme, E. V. Lavrov and J. Weber, *Phys. Rev. B: Condens. Matter Mater. Phys.*, 2005, **72**, 195211.
22 D. C. Look, G. C. Farlow, P. Reunchan, S. Limpijumnong, S. B. Zhang and K. Nordlund, *Phys. Rev. Lett.*, 2005, **95**, 225502.
23 F. F. Lange, *Science*, 1996, **273**, 903–909.
24 D. Andeen, L. Loeffler, N. Padture and F. F. Lange, *J. Cryst. Growth*, 2003, **259**, 103–109.
25 A. Y. L. Sim, G. K. L. Goh, S. Tripathy, D. Andeen and F. F. Lange, *Electrochim. Acta*, 2007, **52**, 2933–2937.
26 W. J. Li, E. W. Shi, W. Z. Zhong and W. Z. Tin, *J. Cryst. Growth*, 1999, **203**, 186.
27 G. K. L. Goh, S. M. Haile, C. G. Levi and F. F. Lange, *J. Mater. Res.*, 2002, **17**, 3168.
28 G. K. L. Goh, F. F. Lange, S. M. Haile and C. G. Levi, *J. Mater. Res.*, 2003, **18**, 338.
29 J. H. Kim, E.-M. Kim, D. Andeen, D. Thomson, S. P. DenBaars and F. F. Lange, *Adv. Funct. Mater.*, 2007, **17**, 463–471.
30 H. Pan, J. B. Yi, J. Y. Lin, Y. P. Feng, J. Ding, L. H. Van and J. H. Yin, *Phys. Rev. Lett.*, 2007, **99**, 127201.
31 J. B. Yi, H. Pan, J. Y. Lin, J. Ding, Y. P. Feng, S. Thongmee, T. Liu, H. Gong and L. Wang, *Adv. Mater.*, 2008, **20**, 1170.
32 W. I. Park, S. J. An, G. C. Yi and H. M. Jang, *J. Mater. Res.*, 2001, **16**, 1358.
33 C. F. Zhang, Z. W. Dong, G. J. You, S. X. Qian, H. Deng, H. Gao, L. P. Yang and Y. Li, *Appl. Phys. Lett.*, 2005, **87**, 051920.
34 R. D. Shannon, *Acta Crystallogr., Sect. A: Cryst. Phys., Diffr., Theor. Gen. Crystallogr.*, 1976, **32**, 751.
35 S. Shet, K.-S. Ahn, Y. F. Yan, T. Deutsh, K. M. Chrustowski, J. Turner, M. Al-Jassim and N. Ravindra, *J. Appl. Phys.*, 2008, **103**, 073504.
36 R. Viswanatha, S. Sapra, S. S. Gupta and B. Satpati, *J. Phys. Chem.*, 2004, **B108**, 6313.
37 D. Chakraborti, J. Narayan and J. T. Prater, *Appl. Phys. Lett.*, 2007, **90**, 062504.
38 K. Sato and H. Katayama-Yoshida, *Jpn. J. Appl. Phys.*, 2000, **39**, L555.
39 X. Feng, *J. Phys.: Condens. Matter*, 2004, **16**, 4251.
40 P. Ágoston and K. Albe, *Phys. Rev. Lett.*, 2009, **103**, 245501.
41 A. Tiwari, M. Snure, D. Kumar and J. T. Abiade, *Appl. Phys. Lett.*, 2008, **92**, 062509.
42 X. L. Wu, G. G. Siu, C. L. Fu and H. C. Ong, *Appl. Phys. Lett.*, 2001, **78**, 2285.
43 D. Li, Y. H. Djurisic, A. B. Leung, Z. T. Liu, M. H. Xie, S. L. Shi, S. J. Xu and W. K. Chan, *Appl. Phys. Lett.*, 2004, **85**, 1601.
44 B. Lin, Z. Fu and Y. Jia, *Appl. Phys. Lett.*, 2001, **79**, 943.
45 N. Ohashi, T. Ishigaki, N. Okada, H. Taguchi, I. Sakaguchi, S. Hishita, T. Sekiguchi and H. Haneda, *J. Appl. Phys.*, 2003, **93**, 6386.
46 Y. B. Zhang, S. Li and G. K. L. Goh, *J. Appl. Phys.*, 2009, **105**, 07C504.
47 N. S. Ramgir, I. S. Mulla and V. K. Pillai, *J. Phys. Chem. B*, 2006, **110**, 3995.
48 C. D. Wagner, D. E. Passoja, H. F. Hillery, T. G. Kinisky, H. A. Six, W. T. Jansen and J. A. Taylor, *J. Vac. Sci. Technol.*, 1982, **21**, 933.
49 E. V. Lavrov, J. Weber, F. Borrnert, C. G. Van der Walle and R. Helbig, *Phys. Rev. B: Condens. Matter Mater. Phys.*, 2002, **66**, 165205.

